Radio Science

RESEARCH ARTICLE
10.1029/2018RS006594

Key Point:
- A novel transition from PCB to a 3-D printed TEM horn antenna with a broadband (4 to 40 GHz) operational bandwidth is presented

Correspondence to:
H. Esteban González,
hesteban@dcom.upv.es

Citation:
Miralles, E., Schoenlinner, B., Belenguer, A., Esteban, H., & Ziegler, V. (2019). A 3-D printed PCB integrated TEM horn antenna. *Radio Science*, *54*, 158–165. https://doi.org/10.1029/2018RS006594

Received 30 MAR 2018
Accepted 31 DEC 2018
Accepted article online 8 JAN 2019
Published online 30 JAN 2019

A 3-D Printed PCB Integrated TEM Horn Antenna

Enrique Miralles[1], Bernhard Schoenlinner[2], Ángel Belenguer[4], Héctor Esteban[3], and Volker Ziegler[1]

[1]Airbus Group Innovations, Taufkirchen, Germany, [2]Airbus Defence and Space, Ulm, Germany, [3]Universitat Politècnica de València, Camino de Vera, s/n, Valencia, Spain, [4]Escuela Politécnica de Cuenca, Campus Universitario, s/n, Cuenca, Spain

Abstract This paper presents a very broadband (5–40 GHz) novel three dimension (3-D) printed Transverse ElectroMagnetic (TEM) horn antenna. It is integrated with a planar Printed Circuit Board and radiates in a perpendicular direction of the Printed Circuit Board. The described antenna provides benefits in terms of cost and size for a two dimensional antenna array. Here the antenna and its corresponding transition to a regular 50 Ω microstrip line through Parallel Plate Waveguide and a 90° bend are presented. Prototypes of back-to-back transitions and antenna are fabricated and measured. The antenna has a return loss below −10 dB and a gain of approximately 10 dBi over the targeted frequency range.

1. Introduction

Three-dimensional (3-D) printing is revolutionizing the industry (Petrick & Simpson, 2013) with many applications for different sectors such as the medical (Zunig et al., 2014), automotive (Local motors, 2017), construction (3DPrint.com. The Voice of 3D Printing/ Additive Manufacturing, 2016), and aeronautic (Tomlin & Meyer, 2011). Some of the benefits of 3-D printing are fast prototyping capability, design flexibility, low material waste, no middleman (from the printer to the user), and the possibility of cost and weight reduction. Over the last years, the scientific community has paid attention to and spent effort on combining this new technology with Radio Frequency (RF) applications. Proof of that is the increasing number of recently published articles related to this topic as, for example, a 3-D printed patch antenna (Liang, Shemelya et al. 2015), a vertical transition on a multilayer printed substrate (Liang, Yu et al. 2015), a multilayer microstrip line (MSL) and a dipole antenna (Shemelya et al., 2015), dielectric reflect arrays (Nayeri et al., 2014), a traditional horn antenna (Garcia et al., 2013), and a lens-antenna (Gianesello et al., 2016).

Multifunctional RF systems (Tavik et al., 2005) provide Size, Weight, and Power reduction compared to conventional systems and often rely on very broadband operation. However, broadband antennas that can conveniently be integrated in Printed Circuit Boards (PCBs), like Tapered Slot Antenna, often radiate in the perpendicular direction of the PCB. If a two-dimensional array is needed then they cannot be integrated in a single PCB and a sandwich configuration with multiple stacked PCBs is required. Accordingly, the costs and the volume of the overall system would increase.

In this work, a 3-D printed Transverse ElectroMagnetic Horn antenna (Ahmed et al., 2016), which can be integrated with PCBs and radiates normal to the PCB plane, is developed, designed, fabricated, and measured. This antenna enables to build a very broadband 2-D antenna array with potential benefits for Size, Weight, and Power and cost.

2. Antenna Concept

Figure 1 depicts a sketch of the antenna and its transition to MSL. The main beam of the antenna radiates in the broadside direction $\hat{z}$ as Figure 1a shows. The antenna is made up of two conductive parts which are fastened together on the top and the bottom of a PCB with a dielectric screw in order to avoid short-circuits (see Figure 1b). Figures 1c and 1d illustrate the bottom view with the transition from MSL to Parallel Plate Waveguide (PPW) and the sideways view with the 90° PPW bend, respectively. To fabricate the two conductive parts with a standard direct machining tool is not possible due to their geometrical complexity. Therefore, 3-D printing is used, although the roughness is relatively high in comparison with other fabrication methods.

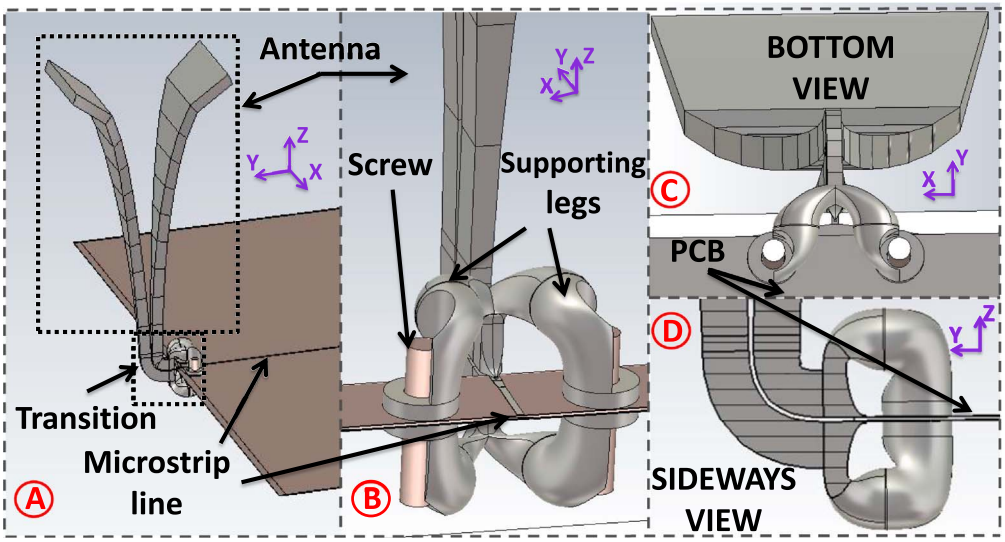

Figure 1. Sketch of the proposed antenna. (a) General view. (b) Focus on the transition. (c) Bottom view. (d) Sideways view. PCB = Printed Circuit Board.

3. MSL to PPW Transition

In this section the designed transition from a MSL to PPW is described.

3.1. Back-to-Back Transition Within a PCB

The selected dielectric material for the PCB has an electrical permittivity ϵ_r of 3.55, loss tangent tan(δ) of 0.0027, and height h of 203 μm. The width of the MSL w_{ms} is 0.422 mm and of the PPW w_{ppw1} is 0.580 mm. They are calculated with the classical Wheeler equations (Wheeler, 1965) to have an impedance of 50 Ω. Both transmission lines are connected via a tapered structure with a length of L_{t1} = 1 mm. The ground plane of the MSL and a strip conductor of the PPW are joined on one face of the dielectric sheet and the other two strips are united on the opposite face (see Figures 2 and 3).

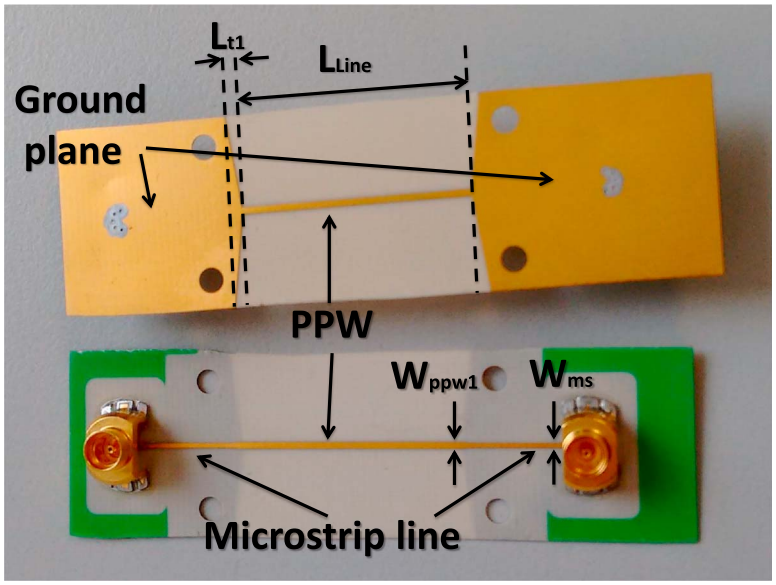

Figure 2. Photography of the back-to-back transition on the Printed Circuit Board with the main geometrical parameters. PPW = Parallel Plate Waveguide.

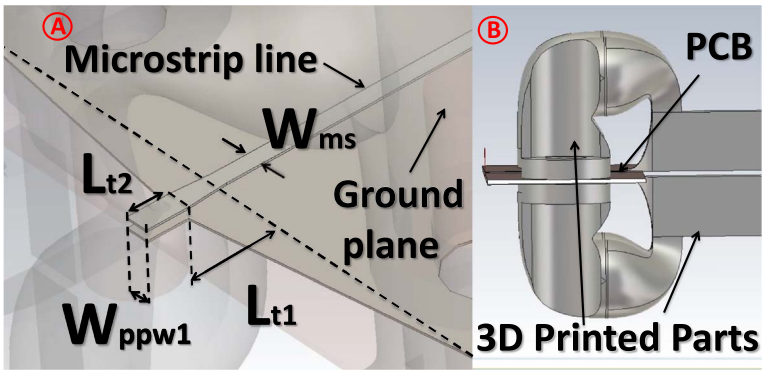

Figure 3. The 3-D sketch of the microstrip line-to-Parallel Plate Waveguide transition on the PCB. (a) Main geometrical parameters. (b) General view. PCB = Printed Circuit Board.

A back-to-back PCB transition from a microstrip line to PPW (filled with dielectric material) is fabricated and tested. It must be noticed that this transition does not include any 3-D printed part since it is only an intermediate step. The transition has a length L_{Line} of 20 mm.

Figure 4 depicts the simulated and measured S-parameters of the described transition. Computer Simulation Technology commercial electromagnetic solver has been used for the simulations. The simulation and the measurement of the S-parameters present good agreement. The reflection is less than −10 dB almost over the whole frequency range of interest. This is an acceptable value considering that the measured back-to-back transition has two transitions and its influence in the final structure is approximately 6 dB less. Moreover the short tapered transition $L_{t1} = 1$ mm produces small mismatches, which are responsible for the small resonances that the Insertion Loss (IL) plot shows. These small resonances can be reduced by lengthening the tapered structure. As a consequence, the transition would become larger.

3.2. Back-to-Back Transition Including a 3-D Printed Structure

A PPW with a length of $L_{t2} = 1$ mm is included, in order to connect the 3-D printed parts, which have a width of $w_{ppw2} = 1.33$ mm (see Figure 5). The remaining air gap between plates $S_{gap} = h + 2t$ is 0.273 mm, where $t = 0.035$ mm is the thickness of the metal layer on the PCB.

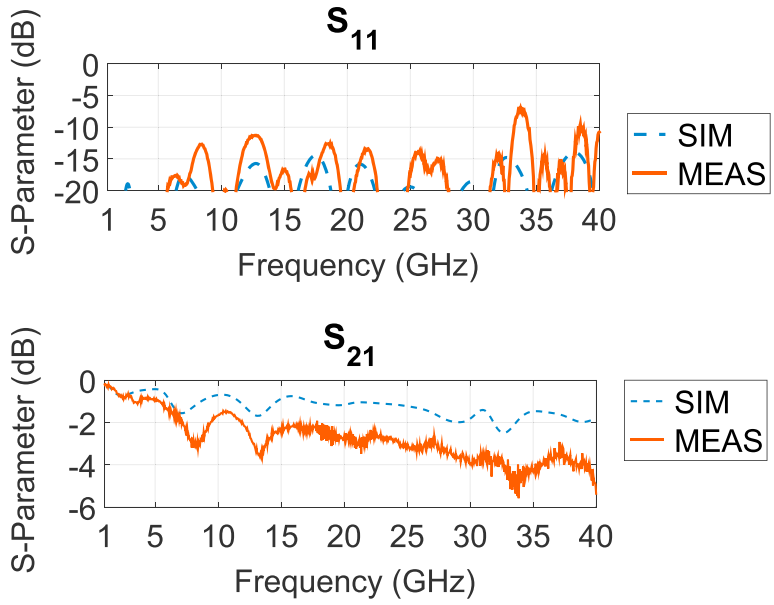

Figure 4. Simulated and measured S-parameters of the back-to-back PCB transition. PPW = Parallel Plate Waveguide; PCB = Printed Circuit Board.

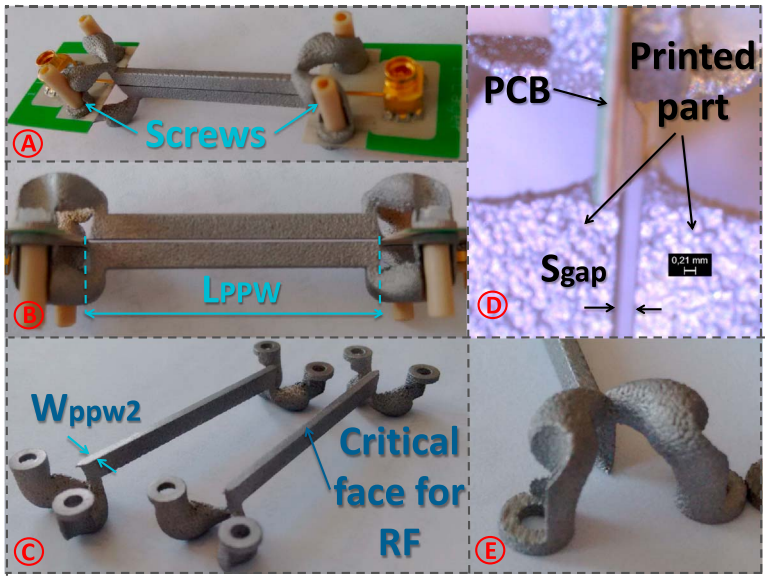

Figure 5. Picture of the back-to-back transition without 90° bends. (a) Plastic screws. (b) Sideways view showing L_{ppw} and w_{ppw2}. (c) Unscrewed parts showing the critical face for RF. (d) Microscope view showing S_{gap}. (e) General view of the supporting legs. PPW = Parallel Plate Waveguide; PCB = Printed Circuit Board; RF = Radio Frequency.

The PPW parts are printed in AlSi10Mg (Aluminum alloy with conductivity between $\sigma = 16$ and21 MS/m) with an accuracy of ± 100 μm with a EOS M270 machine. It operates with Direct Metal Laser Sintering technology. However, more accurate results are achieved depending on the shape and printing position of the part. A back-to-back transition is printed with a length of $L_{ppw} = 33$ mm (see Figure 5). The air gap is measured with a microscope on the PCB to be $S_{gap} = 0.30 \pm 0.01$ mm. In this case, the two faces which form the PPW, which are critical for the RF performance, are printed on top of a flat surface, therefore the measured accuracy is better than ± 100 μm.

The simulation and the measurement of the S-parameters present good agreement (see Figure 6). The reflection is less than -5 dB from 5–40 GHz. This is an acceptable value considering that the measured back-to-back transition has two transitions and its influence in the final antenna is approximately 6 dB

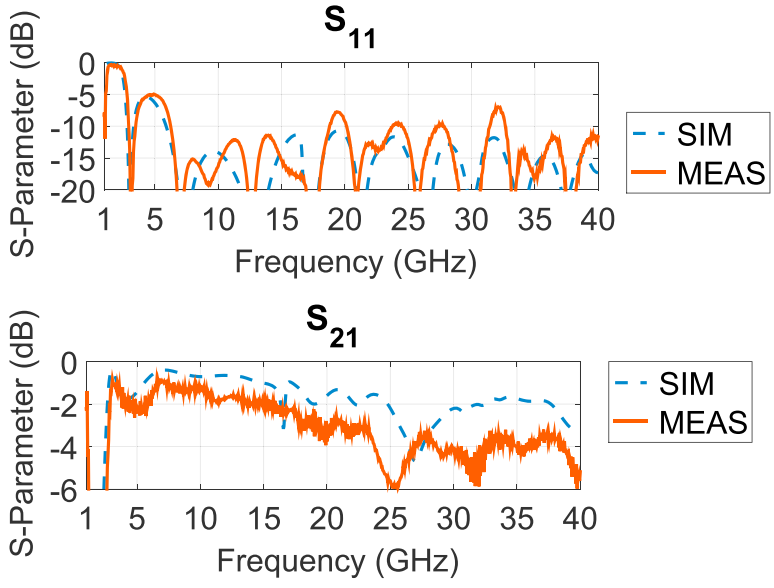

Figure 6. Simulated and measured S-parameters of the back-to-back transition without bends.

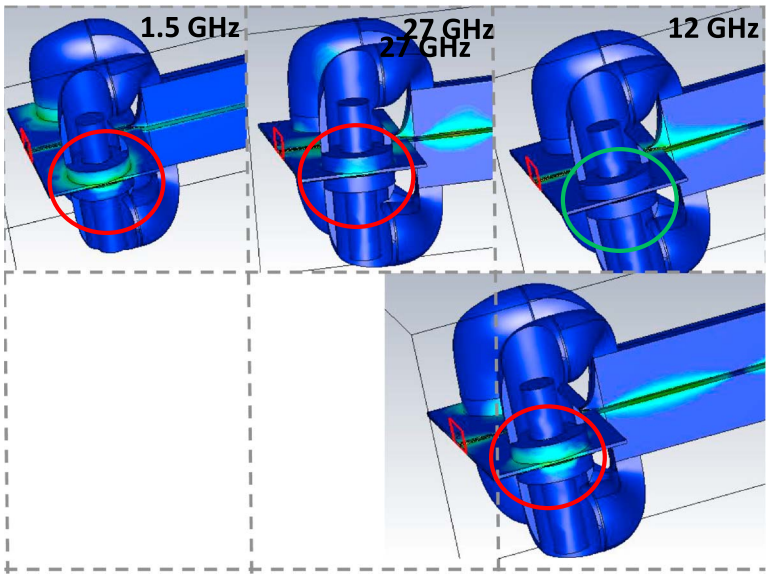

Figure 7. Simulated absolute value of the E-Field at 1.5, 27, and 12 GHz. The red circles indicate the supporting legs which excite resonant modes at 1.5 and 27 GHz. The green circle indicates the supporting legs which do not excite resonant modes at 12 GHz.

less. The IL is a value between −2 and −4 dB in the targeted frequency range. The metallic supporting legs generate resonances (see Figure 7).

3.3. Back-to-Back 3-D Printed Transition Including 90° Bends

Two 90° bends are added to the previous transition as Figure 8 depicts. As a consequence, the shape is more complex and it cannot be printed on a flat surface. Thus, a worsening of the accuracy, especially in the bends, is expected. The air gap is measured within the straight section to be $S_{gap1} = 0.39 \pm 0.03$ mm, at its minimum to be $S_{gap2} = 0.13$ mm and at its maximum to be $S_{gap3} = 0.46$ mm. Hence, impedance variations and higher roughness (Holloway & Kuester, 2000) exist.

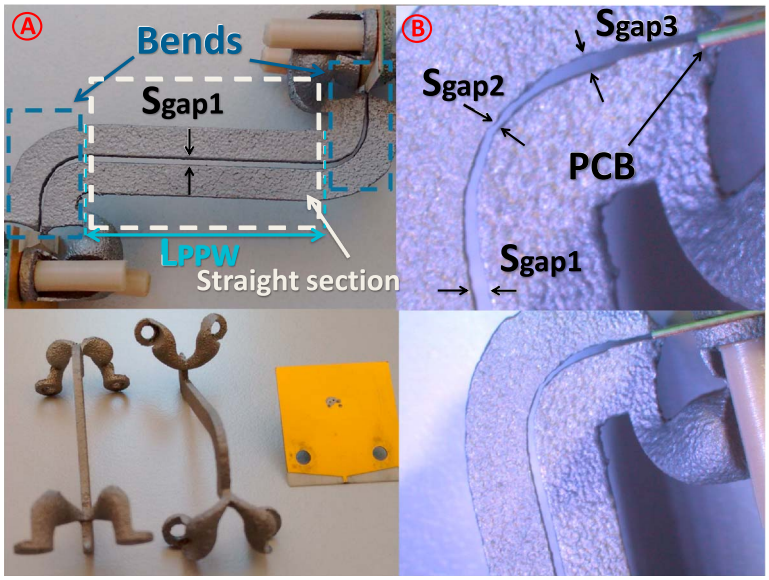

Figure 8. Picture of the back-to-back transition with 90° bends. (a) General view. (b) Microscope view. PPW = Parallel Plate Waveguide; PCB = Printed Circuit Board.

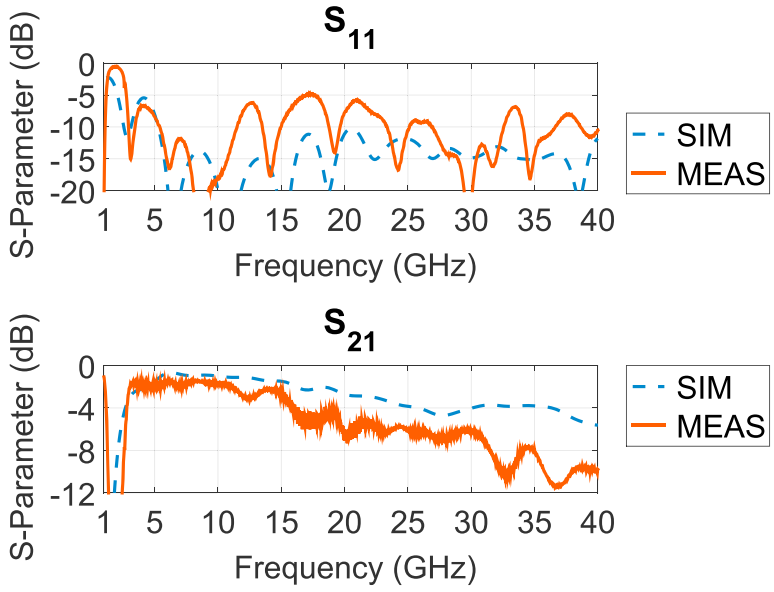

Figure 9. Simulated and measured S-parameters of the transition with bends.

In general, the measured S-parameters fit quite well with the simulation (see Figure 9). However, because of the mismatch introduced by fabrication tolerances, particularly in the bends, the return loss (RL) deteriorates, especially between 13 and 22 GHz.

Nevertheless, the RL still presents a value below −5 dB over the targeted frequency band. The IL is between −3 and −10 dB from 5 to 40 GHz. It presents higher losses due to higher roughness in the entire structure and a longer length, since each bend is 7.58 mm long.

4. Antenna Results

A Transverse ElectroMagnetic horn antenna based on the transition and the 90° bend presented above is designed following a published design procedure (Malherbe, 2012; see Figure 10). The aperture of the antenna is 42×30 mm^2 and its length is $L_a = 85.5$ mm. The antenna is manufactured in the same manner as the PPW parts of the back-to-back transition. That is, with the EOS M270 machine and AlSi10Mg (Alu-

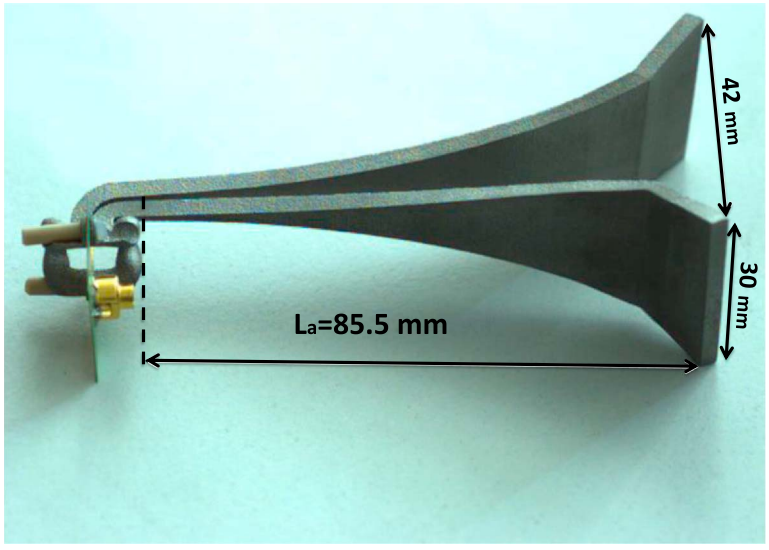

Figure 10. Photography of the final 3-D Printed Antenna.

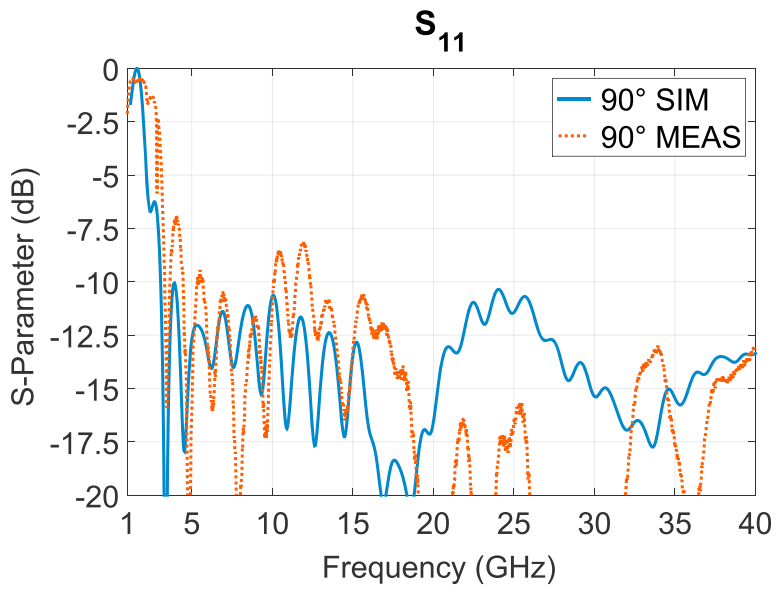

Figure 11. Simulated and measured S_{11} of the antennas with 90° bend.

minum alloy with conductivity between $\sigma = 16$–21 MS/m). In order to measure the matching and gain of the antenna, it has been fixed to a foam surface, and an RF link with a known test antenna probe used as receiver has been established. The measured RL fits rather well the simulation (see Figure 11). It is below −10 dB for almost the whole targeted frequency range.

The roughness of the PPW and the fabrication tolerances explain the small differences between the measured and simulated RL.

An antenna without bend has also been fabricated and measured in order to examine the effect of the bend in the gain (see Figure 12). The antennas (notably the one without the 90° bend) fit well with the simulation. The higher roughness and the higher inaccuracy in the PPW of the antenna with the 90° bend lead to higher losses and thus, lower gain.

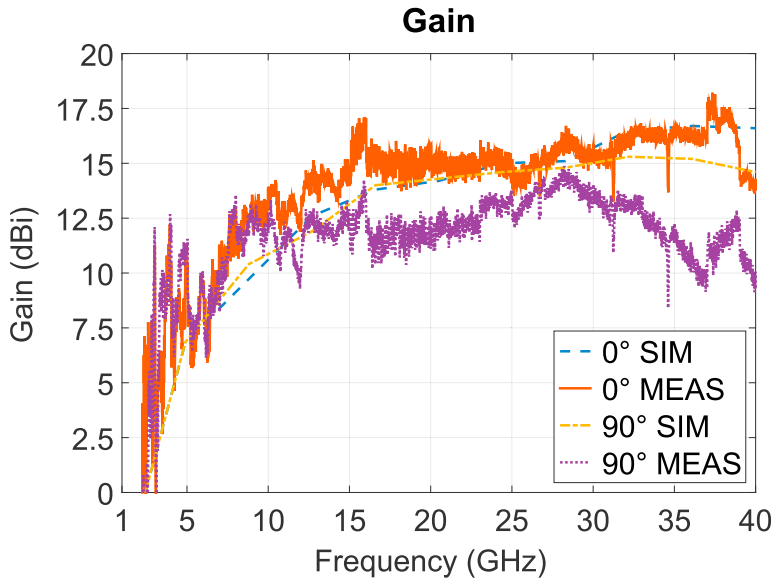

Figure 12. Simulated and measured gain of the antennas with and without bend.

5. Conclusion

This article presents a novel 3-D printed and integrable-with-PCB broadband antenna which radiates in the direction perpendicular to the PCB. The antenna and its transition have been measured with good results in terms of gain (approximatively 10 dbi) and RL (below −10 dB) over a wide frequency range (from 5 to 40 GHz). This results could be further improved by selecting a thicker substrate, in this manner, the fabrication tolerances would affect less the antenna performance. However, a too thick substrate would restrict the operational bandwidth of the antenna, since the cutoff frequency of high order modes in a microstrip line is inversely proportional to its height. In addition, the surface roughness can be improved by using a surface finish treatment.

Acknowledgments
All data necessary to understand, evaluate, replicate, and build upon this research have been included in this paper. No additional data need to be made available.

References

Ahmed, A., Zhang, Y., Burns, D., Huston, D., & Xia, T. (2016). "Design of UWB antenna for air-coupled impulse ground-penetrating radar". *IEEE Geoscience and Remote Sensing Letters*, *13*(1), 92–96.

Garcia, C. R., Rumpf, R. C., Tsang, H. H., & Barton, J. H. (2013). "Effects of extreme surface roughness on 3D printed horn antenna". *Electronics Letters*, *49*(12), 734–736.

Gianesello, F., Bisognin, A., Titz, D., Luxey, C., Fernandes, C. A., Costa, J. R., & Gloria, D. (2016). "3D printing technology: Enabling innovative International Workshop on Antenna Technology (iWAT) (pp. 55–56). Cocoa Beach, FL.

Holloway, C. L., & Kuester, E. F. (2000). "Power loss associated with conducting and superconducting rough interfaces". *IEEE Transactions on Microwave Theory and Techniques*, *48*(10), 1601–1610.

Liang, M., Shemelya, C., MacDonald, E., Wicker, R., & Xin, H. (2015). "3-D printed microwave patch antenna via fused deposition method and ultrasonic wire mesh embedding technique". *IEEE Antennas and Wireless Propagation Letters*, *14*, 1346–1349.

Liang, M., Yu, X., Shemelya, C., MacDonald, E., & Xin, H. (2015). "3D printed multilayer MSL structure with vertical transition toward integrated systems". In *2015 IEEE MTT-S International Microwave Symposium* (pp. 1–4). Phoenix, AZ.

Local motors (2017). 3D Printed Car Close-up Look, Mouser's Strati @ Westec 2017. Retrieved from https://localmotors.com/3d-printed-car/, Accessed 7 January 2019.

Malherbe, J. A. G. (2012). "Hybrid elliptic TEM horn with symmetric main beam". In *15th International Symposium on 2012 Toulouse in Antenna Technology and Applied Electromagnetics (ANTEM), FR* (pp. 1–4).

Nayeri, P., Liang, M., Sabory-Garcia, R. A., Tuo, M., Yang, F., Gehm, M., et al. (2014). "3D printed dielectric reflectarrays: Low-cost high-gain antennas at sub-millimeter waves". *IEEE Transactions on Antennas and Propagation*, *62*(4), 2000–2008.

Petrick, I. J., & Simpson, T. W. (2013). "3D printing disrupts manufacturing: How economies of one create new rules of competition". *Research-Technology Management*, *56*, 12–16.

Shemelya, C., Zemba, M., Liang, M., Espalin, D., Kief, C., Xin, H., et al. (2015). "3D printing multi-functionality: Embedded RF antennas and components". In *2015 9th European Conference on Antennas and Propagation (EuCAP)* (pp. 1–5). Lisbon.

Tavik, G., Hilterbrick, C., Evins, J., Alter, J., Crnkovich, J. G., de Graaf, J. W., et al. (2005). "The advanced multifunction rf concept". *IEEE Transactions on Microwave Theory and Techniques*, *53*(3), 1009–1020.

Tomlin, M., & Meyer, J. (2011). "Topology optimization of an additive layer manufactured (ALM) aerospace part". In *The 7th Altair Technology Conference 2011* (pp. 1–9).

Wheeler, H. A. (1965). "Transmission-line properties of parallel strips separated by a dielectric sheet". *IEEE Transactions on Microwave Theory and Techniques*, *13*(2), 172–185.

Zunig, J., Katsavelis, D., Peck, J., Stollberg, J., Petrykowski, M., Carson, A., & Fernandez, C. (2014). "Cyborg beast: A low-cost 3d-printed prosthetic hand for children with upper-limb differences". *BMC Research Notes*, *8*, 1.

3DPrint.com. The Voice of 3D Printing/ Additive Manufacturing (2016). 3D printed house. Retrieved from https://3dprint.com/tag/3d-printed-house/, Accessed 7 February 2019.